

PAPER

## The phenomenology of reconnection events in the reversed field pinch

To cite this article: B. Momo *et al* 2020 *Nucl. Fusion* **60** 056023

View the [article online](#) for updates and enhancements.



**IOP | ebooks™**

Bringing together innovative digital publishing with leading authors from the global scientific community.

Start exploring the collection—download the first chapter of every title for free.

# The phenomenology of reconnection events in the reversed field pinch

B. Momo<sup>1</sup> , H. Isliker<sup>2</sup> , R. Cavazzana<sup>1</sup> , M. Zuin<sup>1</sup> , L. Cordaro<sup>1</sup> , D. Lopez-Bruna<sup>3</sup> , E. Martines<sup>1</sup> , I. Predebon<sup>1</sup> , C. Rea<sup>1</sup> , M. Spolaore<sup>1</sup> , L. Vlahos<sup>2</sup>  and P. Zanca<sup>1</sup>

<sup>1</sup> Consorzio RFX (CNR, ENEA, INFN, Università di Padova, Acciaierie Venete), Corso Stati Uniti 4, 35127 Padova, Italy

<sup>2</sup> Astronomy Lab, Dept. of Physics, Aristotle University of Thessaloniki, 541 24 Thessaloniki, Greece

<sup>3</sup> Laboratorio Nacional de Fusión CIEMAT, 28040 Madrid, Spain

E-mail: [barbara.momo@igi.cnr.it](mailto:barbara.momo@igi.cnr.it)

Received 19 December 2019, revised 25 February 2020

Accepted for publication 6 March 2020

Published 23 April 2020



## Abstract

The phenomenology of reconnection events, associated to relaxations in high-current ( $\sim 1.5$  MA) plasmas of the reversed-field pinch device RFX-mod, is shown. Each relaxation event can be described as a series of stages starting in the core and propagating towards the plasma edge. In an initial stage (trigger), the evolution of the  $q$  profile brings resonant layers closer together, allowing for an interaction of the current sheets associated to tearing modes at the respective rational values of  $q$ . The phase locking of the resonant modes then initiates the reconnection process that, once started, changes the magnetic topology bringing the initially helical state to a more chaotic configuration.

Keywords: plasma physics, reconnection, reversed field pinch, fusion plasma

(Some figures may appear in colour only in the online journal)

## 1. Introduction

Magnetic reconnection is the breaking and reconfiguration of magnetic field lines embedded in a plasma, on time scales faster than allowed by microscopic forms of classical dissipation. Through reconnection the plasma relaxes to a state of lower magnetic energy. Part of the magnetic energy can be converted to kinetic energy affecting plasma dynamics, energetics and transport [1]. Energy conversion and topological change are highly linked in the definition of reconnection properties, deeply involved in plasma self-organization and dynamo processes. Reconnection is a basic phenomenon that occurs in almost all magnetized plasmas, including fusion plasmas where sawteeth, tearing modes and related phenomena are commonly found in tokamaks and stellarators (e.g. [2, 3]). Among the latter, reconnection particularly characterizes the plasma dynamics of the reversed-field pinch (RFP) [4], which is the topic of this paper. Large RFPs involve large plasma currents and therefore a large amount of available magnetic energy. RFPs contain multiple reconnection sites associated to a variety of resonant tearing modes that

eventually give rise to a stochastic magnetic field background. For this reason RFPs are well-suited devices to observe reconnection events.

In this paper, the phenomenology of the impulsive and periodic reconnections is analyzed in detail, through an ensemble average of the data from many reconnection events in high plasma current discharges (1.5 MA) in the RFX-mod device. Spatial and temporal scales are invoked as fundamental observables. A brief description of the RFP and of the experimental set up of RFX-mod completes this introduction. The experimental characterization of the reconnection events is given in section 2, where the evolution of the plasma parameters and magnetic measurements is shown to follow a sequence of temporally-separated stages. In section 3 a model for magnetic topology reconstruction is proposed to follow the onset and evolution of the reconnection process. Indeed, it will be shown how a possible trigger can be identified with geometrical properties of the plasma, and especially with the distance between intense current sheets. Finally, some discussions in section 4 and a brief summary of main points of the paper in section 5 conclude the paper.

### 1.1. RFP equilibria

Contrary to tokamaks and stellarators, in the RFP most of the magnetic field is produced by currents flowing in the plasma, so that self-organization plays an important role [5]. The RFP can be considered as an overdriven tokamak, with reversal of the toroidal field at the edge. In particular, differently from the tokamak, where the toroidal field ( $B_\varphi$ ) produced by external coils is largely dominant over the poloidal field ( $B_\theta$ ) produced by the plasma current, in the RFP the two magnetic field components are comparable. The ordering  $B_\varphi(0) > \langle B_\varphi \rangle \sim B_\theta(a) \gg B_\varphi(a)$  holds, being  $B_\varphi(0)$  its value on the magnetic axis,  $a$  the minor radius of the plasma, and  $\langle \dots \rangle$  the volume average. As a result, magnetic field lines are almost toroidal in the core and poloidal at the edge, and the safety factor has a spatial profile decreasing from the core outwards, with a core value  $q(0) \ll 1$ . Such a  $q$  profile, below the Kruskal-Shafranov stability criterion, leads to the growth and saturation of several resonant magnetohydrodynamic (MHD) instabilities and is the reason why the RFP configuration was considered intrinsically unstable. Tearing mode instabilities were considered as an unavoidable ingredient of the dynamo self-organization process necessary for the sustainment of the configuration in time, through the  $\langle \tilde{v} \times \tilde{B} \rangle$  term in the resistive Ohm's law.  $\tilde{v}$  and  $\tilde{B}$  are the fluctuating components of fluid velocity and magnetic field, respectively, and  $\langle \dots \rangle$  indicates ensemble averaging [5]. The occurrence of several MHD modes resonating on different plasma layers gives rise to overlapping magnetic islands, which result in a chaotic region extending over most of the plasma volume, where the magnetic surfaces are destroyed and the confinement level is poor. This condition is generally dubbed as the multiple-helicity (MH) state [4].

Along with the MH configuration where the dynamo is produced by the activity of many tearing modes having a more or less constant saturated amplitude, non-linear MHD simulations predicted that one single mode is in principle enough to sustain the RFP configuration, through the so-called laminar dynamo (see [6]–[9]). The transition from MH to single helicity states (SH) is continuous and takes place through a stage where the plasma shows intermittent occurrences of MH states from a quasi-single helicity state (QSH), characterized by a single mode dominating the magnetic spectrum over secondary modes with low but non-negligible amplitude [10].

Transitions to QSH states have been observed indeed in all major RFP devices and can be either spontaneous, externally controlled by the application of magnetic perturbations with external coils or the result of pulsed poloidal current drive (PPCD) experiments (see e.g. QSH discover in RFX-mod [11], MST [12], [13], EXTRAP T2R [14] and TPE [15], and the overview [16]). Spontaneous QSH states have been experimentally observed in RFX-mod at high plasma current ( $> 1$  MA), which seems to play as ruling parameter. In particular, the high-current experiments (up to 2 MA) performed in RFX-mod have shown robust transitions to QSH, a state that becomes more persistent and purer as the plasma current is raised [17]. The dominant mode is experimentally related to the innermost resonant tearing mode. Below a certain threshold in the amplitude of the dominant mode, QSH

states feature a well-confined magnetic island with the periodicity of the dominant mode in the plasma core. These states are dubbed double axis state (DAX). Above that threshold, the configuration self-organizes into a new MHD equilibrium named SHAX, in which a helical structure without X-point dominates in the core, thus exhibiting a ‘single helical axis’ corresponding to the island O-point [18]–[20]. Experimentally, SHAX states exhibit steep core electron temperature gradients, enclosing thermal structure, even in presence of non-vanishing secondary modes [21, 22]. Internal transport barriers were shown to be linked to the shape of the safety factor profile in helical states [23]. QSH states can last for several energy confinement times, but are only intermittent phases, and frequent back-transitions to MH states are observed, associated to almost cyclic, spontaneous and discrete rearrangements of the magnetic-field topology (discrete relaxations events—DREs), similar to what is found in MHD simulations [10].

Plasma relaxations are associated to toroidal flux generation, which would otherwise decay on a resistive time scale. During relaxations the magnetic topology changes with the conversion of helical flux to toroidal flux through a reconnection process. The latter is governed by the current density distribution: the plasma can be thought as electric current circuits at various radii interacting among themselves. During reconnection a global radial re-arrangement of plasma currents and the amplification of parallel currents in some precise plasma region bring on the re-arrangement of the plasma shape itself. Since the initial phase of the reconnections, a localized helical kink-like deformation is visible due to the phase-locking of the resonant tearing modes in the region where many modes with poloidal number  $m = 1$  have their maxima. Moreover, the deformation induced by the locking in phase of the toroidally coupled  $m = 0$  modes modifies the plasma radius, shrinking and enlarging the plasma cross section in the same toroidal region [24]. Phase-locking of the secondary modes corresponds to toroidally localized burst of MHD activity in Fourier space, and produces a toroidally asymmetric region of enhanced plasma-wall interaction and particle transport [25]. The toroidal angle where the perturbation occurs in subsequent DREs is randomly distributed [17], and corresponds to the reconnection toroidal starting point [26]. In high plasma current discharges, reconnection brings the system from QSH, where a clear helical deformation of the plasma column can be seen, to more axis-symmetric MH states; whereas in low plasma current discharges the magnetic topology remains in the MH configuration with less abrupt changes. The study of relaxation events in low-current plasmas, with additional information from insertable probes, showed the formation of an edge current sheet aligned with the magnetic field [27] in agreement with that theoretically found in [4]. On the other side, back and forth passage from QSH to MH states at high plasma currents provides a privileged experimental framework for the observation of reconnection processes. In the following we define spatial and temporal scales of the DREs, using the terms DREs or reconnection events almost indistinctly.

## 1.2. RFX-mod and the experimental set up

RFX-mod [28] is a toroidal device with circular shape,  $R_0 = 2$  m and  $a = 0.459$  m ( $R_0$  and  $a$  being major and minor radii, respectively), that can work both as low plasma current tokamak [29] and as reversed field pinch. In the RFP configuration RFX-mod can reach high plasma current levels up to 2 MA, by virtue of its complex real-time feedback control system, made of 192 independently fed, saddle coils, fully covering the machine [30]–[34]. The enhanced control capability gave access to the QSH improved confinement regimes in high current RFP plasmas [35]. The helical periodicity during QSH states coincides with the periodicity of the innermost resonant mode, i.e. the  $m = 1, n = 7$  in RFX-mod. The principal secondary modes, that are usually seen to increase first and with higher amplitudes, are those related to the successive  $n = 8, 9, 10, \dots$  harmonics.

The determination of the MHD activity is based on a system of edge in-vessel coils, which constitute part of the ISIS (Integrated System of Internal Sensors) diagnostic system, measuring the time derivative of the three components of the magnetic field fluctuations at the edge (at  $r = a$ ), and along the full toroidal angle [36]. The part of the ISIS diagnostic devoted to measuring the toroidal magnetic field component  $B_\varphi(a)$  is made of 48 probes equally distributed along the toroidal direction at two different poloidal angles ( $\approx 70^\circ$  and  $\approx 250^\circ$ ). The two toroidal arrays, being located at distinct but fixed poloidal locations, allow for the discrimination of the odd and even poloidal components of the signals (in RFX-mod known to correspond mainly to  $m = 1$  and  $m = 0$ ), by evaluating the half-difference and half-sum of the signals in opposite poloidal positions, respectively.

An example of a signal deduced after time-integration to obtain the time behavior of  $B_\varphi(a)$  is given in figure 1 along with the time trace of the plasma current  $I_p$  for a typical high-current RFP discharge (#29255). The signal is characterized by fluctuations at various scales, both in time and amplitude. The largest ones are associated with a global re-arrangement of the magnetic field topology. Figure 2 is a color-coded contour plot showing a detail of what happens on the whole set of 48 signals in the selected time interval indicated by the dotted lines in figure 1. The largest, impulsive, generation of magnetic fluctuations occurs at a given toroidal angle, due to the locking in phase of the biggest MHD modes. This can be inferred from the time traces of two single probes also plotted in figure 2, which correspond to different toroidal angles: it is seen that the event around  $t = 0.173$  s is more pronounced near  $\varphi = 174^\circ$ , while the event near  $t = 0.192$  s is more clearly detected by the probe at  $\varphi = 46^\circ$ .

## 2. Experimental results in high plasma current discharges

### 2.1. General features of discrete relaxation events

The re-arrangement of the magnetic topology during the DREs observed in the RFP plasma leaves its most clear signature

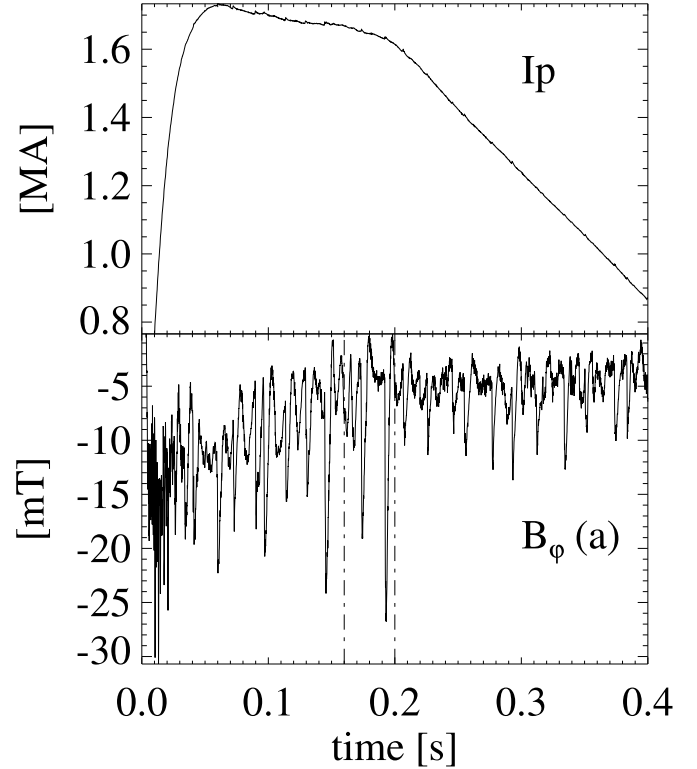


**Figure 1.** Typical high-plasma-current RFX-mod discharge #29255. Top: time trace of the plasma current  $I_p$ . Bottom: a single signal from one of the 48 coils of the ISIS toroidal array.

with a “crash” of the reversal parameter (toroidal magnetic field at the plasma boundary/volume average toroidal field)  $F = B_\varphi(a)/\langle B_\varphi \rangle$  time trace, but of course affects other global electromagnetic quantities of the plasma. The most relevant ones are reported in figure 3, where the time evolution of reversal parameter  $F$ , plasma internal inductance  $L$ , plasma current  $I_p$ , toroidal loop voltage  $V_t$ , average toroidal magnetic field  $\langle B_\varphi \rangle$  and poloidal loop voltage  $V_p$  are plotted using the data coming from the same discharge of figures 1 and 2 during its flat-top. Vertical bands highlight the features that accompany each major event, which are typical of DREs in high plasma current discharges at shallow  $F$  ( $F \lesssim 0$ ).

As already said, DREs are associated with toroidal flux generation, and more generally to a re-arrangement of the current density distribution  $J$  in the plasma.

In RFP configuration the paramagnetic structure, which intensifies the toroidal field toward the plasma center, becomes the dominant term for the equilibrium and dwarfs the diamagnetic contribution due to the pressure gradient, which in turn becomes negligible. Thus, in this context, the experimental plasmas can be well described using the *force free* approximation ( $J \approx J_\parallel$ ).

Using this assumption, the zeroth-order MHD equilibrium field  $\mathbf{B}$  can be reconstructed using the method in [37]: the *force free* approximation is stated in the MHD force equation as  $\mathbf{J} \times \mathbf{B} = 0$ . This relation implies a proportionality relation between  $\mathbf{J}$  and  $\mathbf{B}$  (or  $\mathbf{J} = \lambda \mathbf{B}$ ) and the following form for the Ampere’s law:

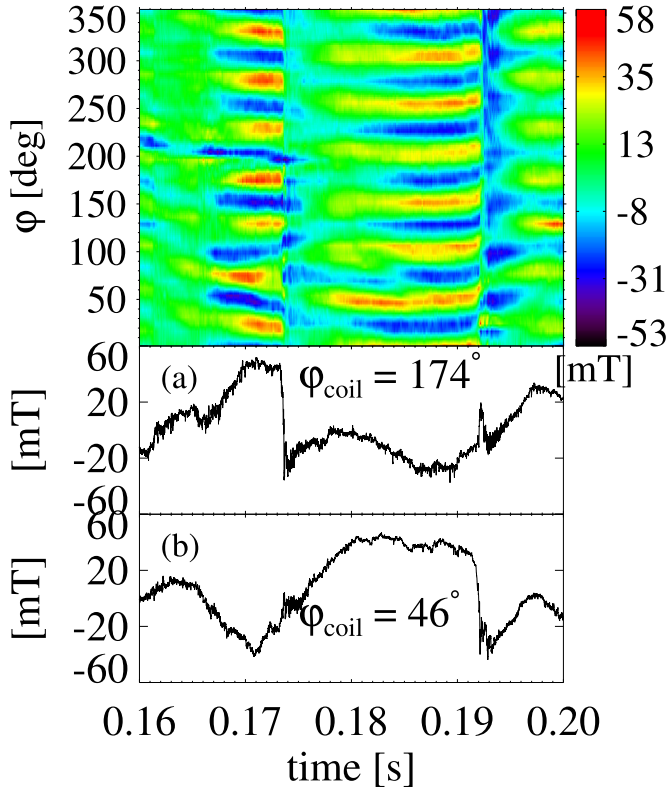


**Figure 2.** RFX-mod discharge #29255. Top: contour plot of the toroidal magnetic field measurements from the 48 ISIS coils along the toroidal angle  $\varphi$ , in the time interval indicated by the two dashed lines in figure 1. Bottom: plot of two single probe signals corresponding to toroidal locations  $\varphi \sim 174^\circ$  (a) and  $\varphi \sim 46^\circ$  (b).

$$\nabla \times \mathbf{B} = \lambda \mathbf{B}. \quad (1)$$

Choosing for  $\lambda(r)$  the parametrization:

$$\lambda(r) = \lambda_0 \left[ 1 - \left( \frac{r}{a} \right)^\alpha \right] \quad (2)$$

the experimental equilibrium is recovered by finding the unique couple of parameters  $(\alpha, \lambda_0)$  defining the solution of equation (1) that matches the two bounding values obtained from the magnetic measurements  $B_\varphi(a)/B_\theta(a)$  and  $\langle B_\varphi \rangle$ .

The common definition of the inductance  $L$  (figure 3(b)) used for tokamak configuration [38] cannot be straightforwardly applied to the RFP and deserves some discussion [39]. The RFP has a strongly screwed current distribution. In general the value of  $L$  depends on the magnetic field self generated by the plasma  $B^*$ , which can be derived by simply subtracting from the total equilibrium field  $B_{\text{tot}}$  the external field generated by magnetic coils  $B_{\text{ext}}$ , so that  $B^* = B_{\text{tot}} - B_{\text{ext}}$ . The plasma internal inductance  $L$  can be then derived from the self generated magnetic energy:

$$W^* = \int \frac{B^{*2}}{2\mu_0} dV = \frac{1}{2} L I_p^2 \quad (3)$$

For both tokamak and RFPs,  $B_{\text{ext}} = B_\varphi(a)$ . In the case of a tokamak the toroidal field is entirely generated from outside and only the poloidal component  $B_{\text{pol}}$  is used to calculate

$L$ . In the RFP the toroidal field is mostly self-generated and becomes an essential part of the definition of  $L$ . In the cases considered in this paper of shallow  $F$  discharges ( $B_\varphi(a) \simeq 0$ ), the MHD equilibrium magnetic field almost coincides with the self-generated field  $B^* \simeq B_{\text{tot}}$  [40]. Being  $L$  related to the integral of the magnetic field on a given plasma volume, an increasing of  $L$  corresponds to a peaking of the current density toward the center, whereas its reduction corresponds to a flattening of the current density profile. Thus even though the current densities are not measured directly in the bulk plasma, the time evolution of the plasma inductance informs about their redistribution in the whole plasma volume. Then for a continuous current density profile in computing  $B_{\text{tot}}$  (e.g. from equations (1) and (2)),  $dL/dt > 0$  is associated to a process concentrating the currents in the core and  $dL/dt < 0$  to a diffusion towards the plasma edge.

In the absence of internal sources, the toroidal loop voltage  $V_t$  (figure 3(d)) is the sum of the ohmic dissipated power  $RI_p$  plus the terms coming from Faraday's law, taking into account the voltages induced by both the variation of the total plasma current and the change of  $L$  due to the magnetic reconfiguration:

$$V_t = RI_p + L \frac{dI_p}{dt} + I_p \frac{dL}{dt} \quad (4)$$

The generation of toroidal flux during the relaxation event creates an electromotive force in the poloidal direction. Because of the finite impedance of the toroidal field circuits this translates into a sudden current variation on the toroidal coils which opposes the toroidal flux generation and appears in the  $F$  trace as a negative spike (the  $F$  'crash', figure 3(a)). The resulting measured  $V_p \propto -d\langle B_\varphi \rangle/dt$  figure 3(e)–(f) come from the interplay between the field generated by the relaxation and the response of the toroidal circuit.

It is useful reminding that the RFP parallel current density is almost toroidal in the core ( $J_{\parallel, \text{core}} \sim J_\varphi$ ) and poloidal at the edge ( $J_{\parallel, \text{edge}} \sim J_\theta$ ), due to the reversal of the toroidal magnetic field. For this reason, the temporal evolution of the loop voltages may inform on the localization of plasma processes that involve a modification of the  $J_{\parallel}$  profile:  $V_t$  detects processes related to the variation of the toroidal parallel current density component, whereas  $V_p$  sees dynamics characterized by strong poloidal current density component and therefore toroidal flux generation. If the variation of  $V_t$  and  $V_p$  are not simultaneous, the localization of core or edge dynamics is straightforward. However, it is worth noting that we deal with integral measurements, which do not allow us to distinguish between generation and redistribution of the currents in the plasma. Moreover, a net magnetic flux self generation and its associated generated current would imply an additional term on equation (4).

In figure 3(g) the relation between DREs and the MHD mode dynamics is shown: the crash of  $F$  is accompanied by the *crash* of the dominant mode and the growth of secondary modes, by which the plasma undergoes a magnetic topology change, passing from a SHAx to a MH state.

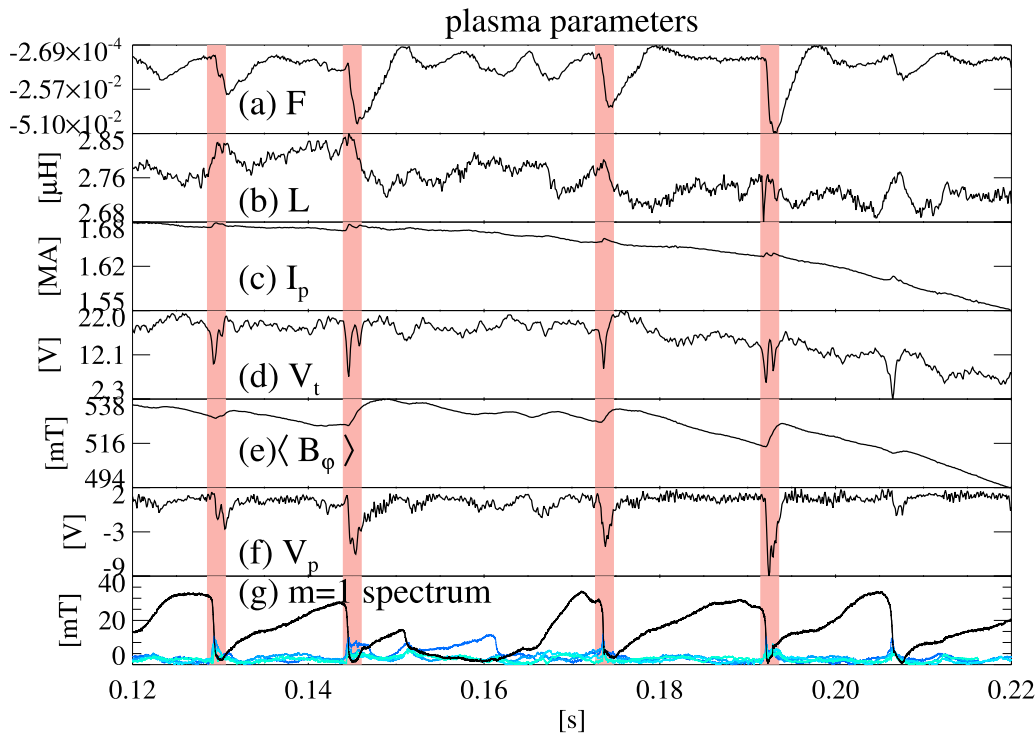


**Figure 3.** RFX-mod discharge #29255. Time evolution of: reversal parameter  $F$ , plasma inductance  $L$ , plasma current  $I_p$ , toroidal loop voltage  $V_t$ , averaged toroidal magnetic field  $\langle B_\phi \rangle$ , poloidal loop voltage  $V_p \propto -dB_\phi/dt$  and MHD modes. Vertical pink bands indicate the main DREs.

The features that accompany relaxation events in high plasma current and shallow  $F$  discharges can be summarized as follow.

- (a) The crash of the edge toroidal field  $B_\phi$  (a) and, correspondingly,  $F$ .
- (b) The rapid change in the plasma inductance  $L$ , with an increasing phase followed by a decreasing one.
- (c) The slight peak in the toroidal plasma current  $I_p$ .
- (d) The crash in the toroidal loop voltage  $V_t$ .
- (e) The sudden increase of the toroidal flux (toroidal field generation).
- (f) The crash in the poloidal loop voltage  $V_p$ .
- (g) The crash of the dominant mode and the growth of secondary modes.

## 2.2. Temporal scales of the reconnection event

With the aim of a more general statistical analysis, an averaged synthetic shot has been defined. Such synthetic shot has been obtained by means of a conditional-averaging process on the various signals over 30 comparable shots in terms of plasma current and equilibrium, for a total of 270 reconnection events, in which both time base and toroidal angle reference systems have been redefined. In particular, based on the observation that the reconnection process appears as a toroidally localized event, the new toroidal angle reference system is defined as to have  $\varphi = 180^\circ$  at the location where, for each single event, the maximum magnetic field perturbation occurs as measured by the fast internal ISIS  $B_\phi$  probes array

located at  $\theta = 250^\circ$ . The time reference for the averaging conditional process is that  $t = 0$  corresponds to the time at which the localized magnetic field perturbation is maximum. From a macroscopic point of view, this is approximately the time corresponding to the minimum of  $F$ . Shot #29255 in figures 1–3 is part of the ensemble and the variability range, in the whole ensemble, of some important plasma parameter is summarized in table 1.

The generation of toroidal flux during the averaged relaxation event is illustrated in figure 4 by the change of the two axisymmetric equilibrium profiles,  $q$  (figure 4(a)) and the parallel current density parameter  $\lambda = \mathbf{J} \cdot \mathbf{B}/B^2 = J_\parallel/B$  figure 4(b), before (black) and after (red) the averaged relaxation event.  $\mathbf{B}$  is the magnetic field previously also called  $B_{\text{tot}}$ , equations (1) and (2) are solved with  $\lambda_0 = 6.47 \pm 0.02 \text{ MA m}^{-2} \text{ T}^{-1}$  and  $\alpha = 5.1 \pm 0.2$ . Reminding that the RFP current density is almost toroidal in the core and poloidal at the edge, the difference between the two  $\lambda$  profiles figure 4(c) clearly shows how the DRE is related to the increase of the almost-poloidal parallel current density near the edge. A representative error bar on the profile curve in figure 4(c) is indicated by a small vertical gray line.

Figure 4 shows the global effect of a DRE considering a large temporal interval around it. A detailed analysis of the temporal evolution shows how DREs can be described in terms of a systematic sequence of well separated stages. All measurements share the same timing and support the idea of a relaxation process that evolves following the  $q$  profile.

Figures 5–8 illustrate the reconnection process for the averaged shot, with the vertical lines indicating the instants chosen

**Table 1.** Plasma parameters in the whole ensemble of the averaged discharge.

plasma parameter	values	plasma parameter	values
Electron temperature $T_e$	850 – 1100 eV	Fuel gas species	Hydrogen
Ion temperature $T_i$	$2/3T_e$	$Z_{eff}^a$	1.5
Plasma density $n_e$	$0.15 - 0.22 n/n_G$	Lundquist number $S^b$	$\sim 10^7$

<sup>a</sup> $Z_{eff}$  is not measured and its value is assumed as suggested in [41].

<sup>b</sup>The value of the  $S$  is computed as in [17], where the Alfvén time is calculated using the equilibrium plasma magnetic field.

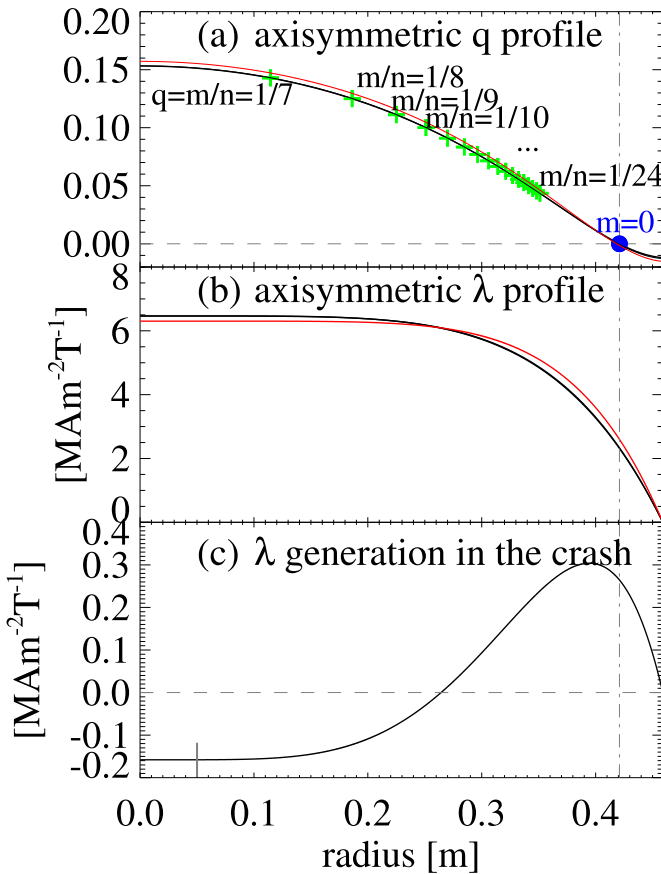


**Figure 4.** Averaged discharge. Axi-symmetric equilibrium profiles at two time instants, before (black) and after (red) the DRE: (a) safety factor profile  $q$ , (b) parallel current density parameter  $\lambda$ , (c) difference between the  $\lambda$  profiles before and after the DRE, showing the parallel current density generated during the reconnection process. A vertical line at  $r \sim 0.42$  m indicates the reversal surface. In (a) green crosses show the main resonant surfaces of the  $m = 1$  spectrum ( $7 \leq n \leq 24$ ) and a blue dot the resonant surface of all the  $m = 0$  modes. In (c) a representative error bar on the profile curve is indicated by a small vertical gray line.

to define the time sequence of the DRE. The quantities  $F$ ,  $L$ ,  $I_p$ ,  $V_t$ ,  $B_\varphi$  and  $V_p$  are presented in figure 5, and the tearing mode dynamics in figures 6–8. In figure 5 representative error bars show the parameter variabilities in the set of discharges of the averaged shot. The qualitative features shown in the averaged shot are shared by the single discharges of the ensemble. We have identified the following characteristic times  $t_i$ ,  $i = 0, \dots, 6$ , to describe the phenomenology with respect to the reference time  $t = 0$ :

- $t = t_0 \simeq -1.4$  ms. *Locking of  $m = 1$  modes.* The abrupt changes in the MHD dynamics and plasma parameters described above is preceded by a slowly-evolving helical SHAx state, during which the global properties of the plasma show only minor changes. At  $t = t_0$  a localized  $m = 1$  magnetic structure arises through an increasing phase-locking of the whole  $m = 1$  spectrum, without affecting mode amplitudes.
- $t = t_1 \simeq -1.0$  ms. *Increase of  $m = 1$  modes in the plasma core.* At  $t_1$  the  $m = 1$ ,  $n = 8$  harmonic amplitude exceeds its averaged value measured for  $t < t_0$ , starting the increase of the  $m = 1$  spectrum which is seen in an intense MHD dynamics mainly related to  $m = 1$  modes resonant in the core ( $n = 8 - 10$ ). At the same time, a quick descent of the toroidal loop voltage  $V_t$  is accompanied by an increase of the plasma inductance  $L$  and of the plasma current  $I_p$ , which is interpreted as a fast amplification of the currents in the core. We refer to  $t = t_1$  as the beginning of the fast stage of the relaxation process, localized in the plasma core.
- $t = t_2 \simeq -0.5$  ms. *Increase of  $m = 1$  modes in the plasma edge.* The plasma inductance is around its maximum ( $dL/dt \simeq 0$ ) and, in accordance with a current density diffusion towards the edge, the plasma is subject to a rapid generation of toroidal flux. The MHD spectra are characterized by strong  $m = 1$ ,  $n > 8$  dynamics, with all the secondary modes now firmly locked in phase. We understand that the  $m = 1$  spectrum is still growing, now involving edge resonant harmonics ( $n > 10$ ) where the reconnecting layer has a strong poloidal component in accordance to the RFP  $q$  profile.
- $t = t_3 \simeq -0.4$  ms. *Conversion to  $m = 0$  reconnection.* At this time we have a minimum of the toroidal loop voltage ( $dV_t/dt = 0$ ). The simultaneous quick descent of  $L$  is interpreted as an equally quick redistribution of the edge (poloidal) current density, indeed occurring together with a strong toroidal flux generation. In  $[t_2, t_3]$  a clear localized  $m = 0$  (mainly  $n = 1$ ) magnetic structure forms at the edge and, on the other hand, at  $t_3$  the total amplitude of the  $m = 1$  modes starts a decreasing phase. We argue that  $m = 0$  reconnection (meaning the existence of a poloidal current sheet) is now taking place at the plasma edge, with a net energy transfer from  $m = 1$  to  $m = 0$  spectra occurring where  $J_{||} = J_\theta$ . This corresponds to the reversal surface, where all  $m = 0$  modes are resonant.
- $t = t_4 \simeq -0.2$  ms. *The  $m = 0$  modes reach their maximum amplitude.* This time corresponds to the minimum of the

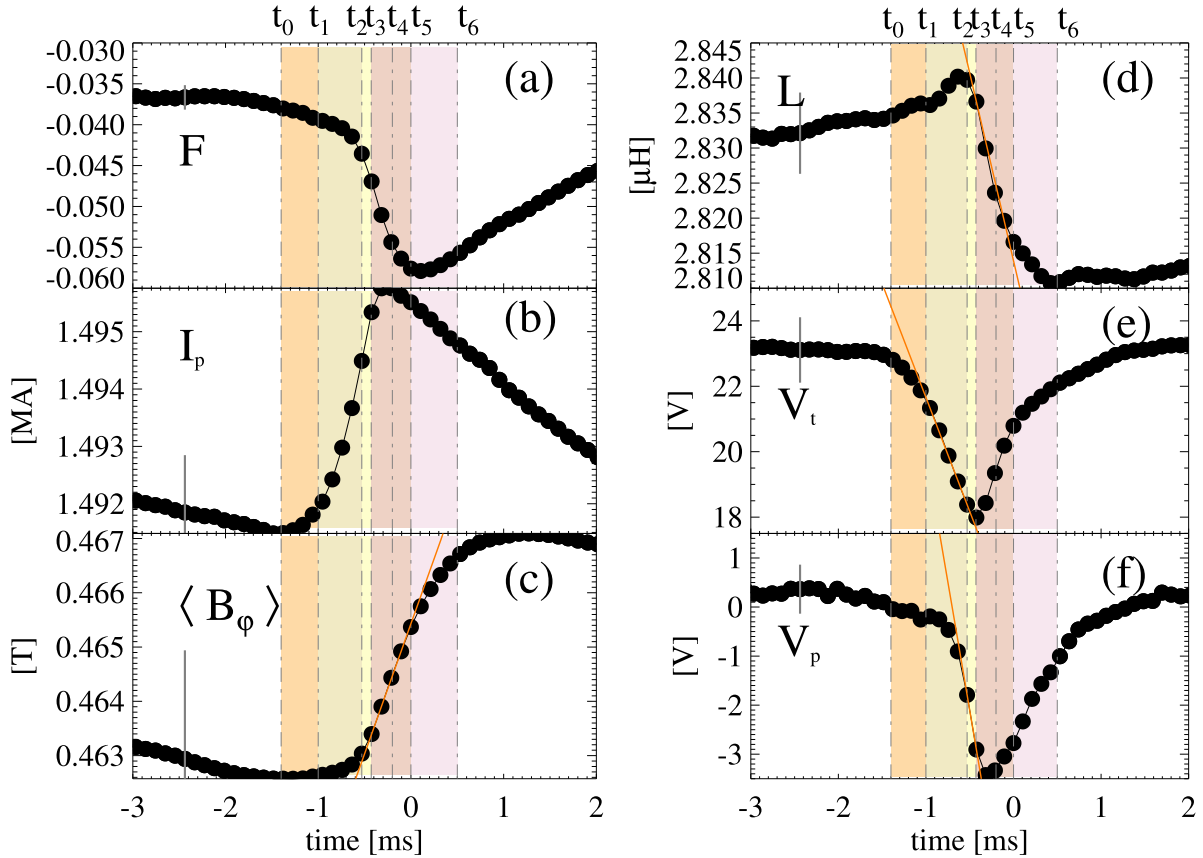


**Figure 5.** Averaged discharge. Time traces of (a) reversal parameter  $F$ , (b) plasma current  $I_p$ , (c) averaged toroidal magnetic field  $\langle B_\phi \rangle$ , (d) plasma inductance  $L$ , (e) toroidal loop voltage  $V_t$  and (f) poloidal loop voltage  $V_p$ , during the DRE. Red lines help in highlighting the change in the slopes. Vertical lines indicate the  $t_i$  ( $i=0, 1, 2, 3, 4, 5, 6$ ) time instants listed in the text. Short gray bars show the parameter variabilities of the set of discharges of the averaged shot.

poloidal loop voltage ( $dV_p/dt=0$ ). There is still a considerable amplification of the edge plasma current density (formation of a localized poloidal current sheet), and the  $m=0$  component now reaches its maximum amplitude.

- f.  $t=t_5 \simeq 0$  ms. *End of the  $m=0$  reconnection stage.* At this time we have the minimum value of  $F$ . The amplitude of the  $m=0$  magnetic structures in the plasma edge starts a decreasing phase and the plasma features a slower current density redistribution.
- g.  $t=t_6 \simeq +0.5$  ms. *End of the reconnection event.* The  $m=0$  magnetic component (and associated current sheet) almost disappears.

The above scheme is summarized in table 2.

As we can see, there is a strict correlation between the tearing mode dynamics and the global current (re)distribution, both evolving following the  $q$  profile. At the beginning, the  $m=1$ ,  $n \geq 8$  modes lock together, then grow in a cascade-like fashion for increasing  $n$  (in  $[t_1, t_3]$ ), with part of their energy being transferred to the  $m=0$  modes (from  $t=t_2$  on). In the time window  $[t_1, t_2]$  (where  $dL/dt > 0$ ) the reconnection process concentrates the currents in the core through the action of the innermost  $m=1$  modes, and a good correlation with the generation of toroidal current can be seen in figure 5(b). From  $t=t_2$ , a flattening of the plasma current density occurs,

with the generation of poloidal current in the edge, where  $m=1$  harmonics with high  $n$ , and the  $m=0$ , are resonant. We remark that, in the RFP,  $J_{\parallel} \simeq J_\phi$  in the core, and  $J_{\parallel} \simeq J_\theta$  in the edge. The growth of the most internal resonating  $m=1$  modes—with current sheets mostly developing in the toroidal direction—is associated to  $J_{\parallel}$  generation in the core, while the subsequent growth of the  $m=1$ , high- $n$  modes and, later,  $m=0$  modes—with current sheets mainly having poloidal component—is related to  $J_{\parallel}$  generation in the edge.

The tearing mode dynamics deserves some more discussion. As we can see in figure 6, the crash of the dominant mode  $n=7$  is accompanied by the growth of secondary modes, figure 6(a). The temporal separation between the growth of the  $m=1$  and  $m=0$  modes, the  $m=1$  spectrum increasing first, is highlighted by coloured bands in the figure. For more clarity, the innermost resonant  $m=1$  secondary modes ( $n=8-10$ ) are plotted separately in figure 6(b): their growth in  $[t_1, t_3]$  is followed by a decreasing phase. At  $t=t_2$ , there is still a strong  $m=1$  dynamics, but not yet  $m=0$ . The interpretation of the evolution of the  $m=0$  spectrum figure 6(c) is somewhat more difficult due to the toroidal coupling between the  $m=0$  and the  $m=1$  (with same  $n$ ) modes [42]. In order to distinguish the origin of the  $m=0$  modes, the  $m=0, n=1$  and  $m=0, n=8$ , are re-plotted in figure 6(d): while the  $m=0, n=8$  mode grows following the same dynamics as the mode  $m=1, n=8$  due

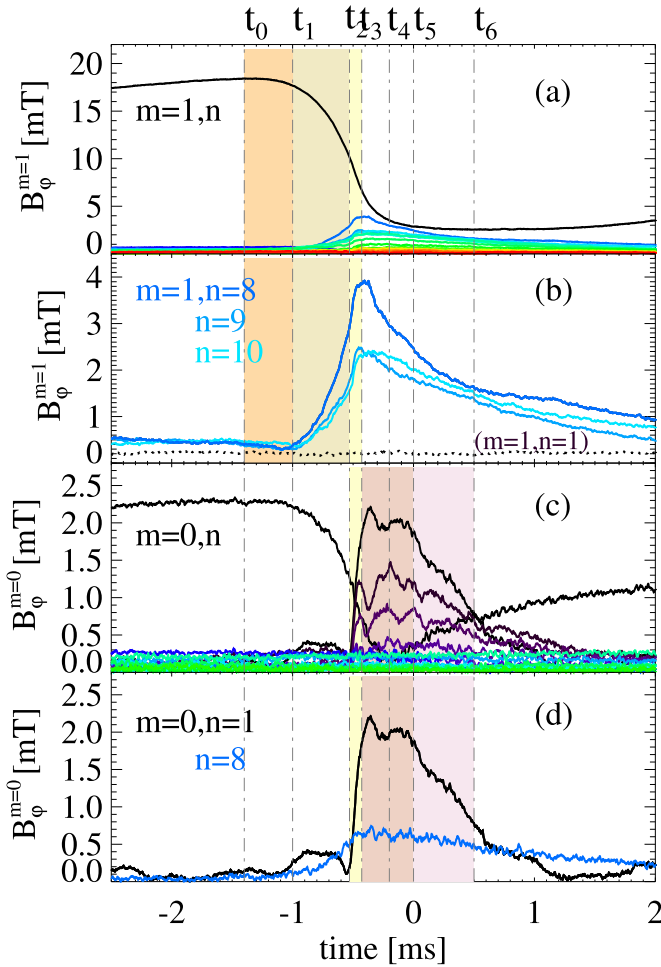


**Figure 6.** Averaged discharge. MHD mode dynamics during the DRE. (a)  $m = 1$  mode spectra, with  $1 \leq n \leq 24$ ; (b) secondary  $m = 1$  modes, with  $8 \leq n \leq 10$ ; (c)  $m = 0$  mode spectra, with  $1 \leq n \leq 24$ ; (d)  $m = 0$  modes, with  $n = 1$  and  $n = 8$ . Vertical lines indicate the  $t_i$  time instants listed in section 2.2.

to toroidal coupling, the mode  $m = 0, n = 1$  quickly grows in  $[t_2, t_3]$ , independently of the  $m = 1$  dynamics.

The short time interval  $[t_2, t_3] \sim 0.1$  ms corresponds to the time in which the  $m = 0$ , low- $n$  structures form. Part of the energy is transferred from  $m = 1$  to  $m = 0$  spectra, as clearly suggested in figure 7(a), where the total amplitudes of the two spectra are plotted (total amplitudes are defined as the square root of the total squared amplitude of the modes with  $n > 0$ , for each spectra, excluding the dominant  $n = 7$  mode). Indeed, the growth and decay mode amplitudes have a dynamics that proceeds following the  $q$  profile.

About this dynamics, limited to the  $m = 1$  spectrum, we remark that the increase of the  $m = 1$  modes from the innermost to the outer ones had already been reported, for individual discharges, in [26, 27] (where the authors speak about energy cascade between the  $m = 1$  modes). In figure 8, we show the evolution of the  $m = 1$  mode amplitudes (in logarithmic scale) for each  $n$  using data from the averaged discharge. The propagation towards higher  $n$  is clearly seen in  $[t_1, t_3]$ .

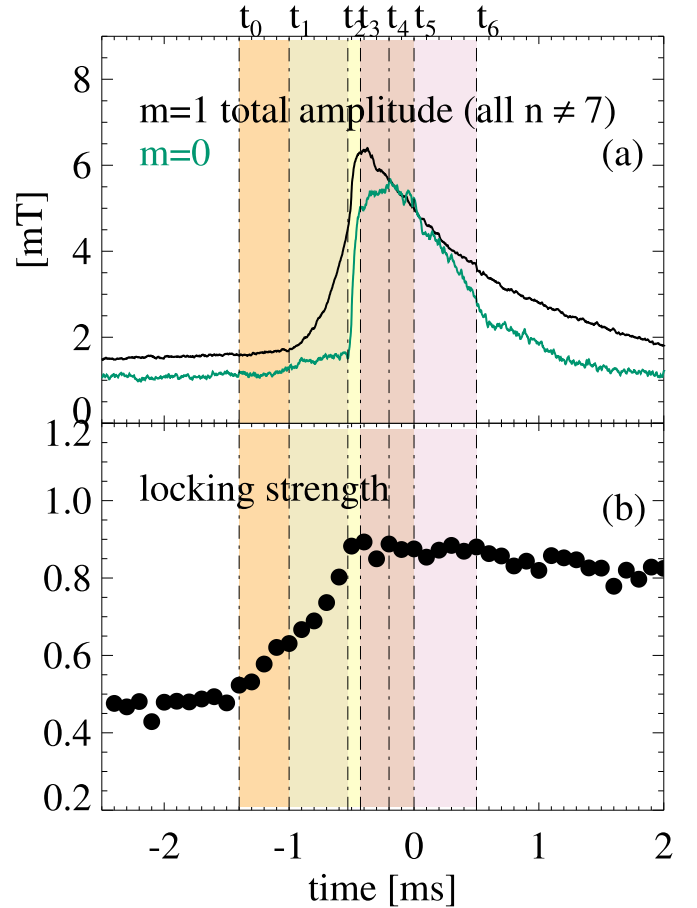


**Figure 7.** Averaged discharge. As a function of time: (a) total amplitude of the  $m = 1$  (black) and  $m = 0$  (green) modes—the latter multiplied by 2 – considering the modes with  $1 \leq n \leq 24$ , for each spectrum, excluding the dominant  $n = 7$  mode; (b) maximum value of the locking strength at  $r = a$ , for the  $m = 1, n \geq 8$  modes. Vertical lines indicate the  $t_i$  time instants listed in section 2.2.

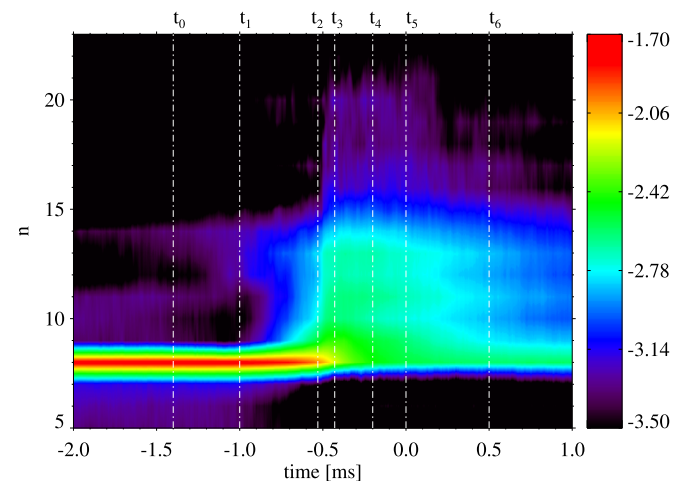


**Figure 8.** Averaged discharge. Time evolution of the  $m = 1, n$  mode amplitudes of  $B_\varphi(a)$  (logarithmic scale). Vertical lines indicate the  $t_i$  time instants listed in section 2.2.

As already said, the fast dynamics related to  $m = 1$  and  $m = 0$  secondary modes is preceded by a slow stage in which

**Table 2.** Summary of the  $t_i$  time instants listed in section 2.2.

$t_i$	(ms)	Brief description
$t < t_0$	$< -1.4$ ms	Trigger of the DRE: approaching of resonant current layers in the plasma core (see section 3.2).
$t_0$	$-1.4$ ms	Initial slowly evolving stage: phase locking of $m = 1$ modes.
$t_1$	$-1.0$ ms	Beginning of fast evolving stages, with the growth of core resonant $m = 1$ modes.
$t_2$	$-0.5$ ms	A poloidal component of $J_{\parallel}$ starts to form, which involves edge resonant $m = 1$ modes.
$t_3$	$-0.4$ ms	The reconnection process involves $m = 0$ modes, resonant on the reversal surface.
$t_4$	$-0.2$ ms	The $m = 0$ modes reach their maximum amplitude.
$t_5$	$0.0$ ms	End of the fast stages of the reconnection process.
$t_6$	$+0.5$ ms	The $m = 0$ modes almost disappears

their several  $n$  components start to phase-lock in some position. The phase-locking is quantified through the *locking strength*  $\sigma$  of the  $m = 1$  modes with  $n \geq 8$  ( $8 \leq n \leq 24$  in figure 7(b)), a parameter ranging from  $\sigma = 1$  when all the considered secondary modes are in phase in some toroidal position, to  $\sigma = 0$  when the phase relation among them is lost [43]. During phase-locking of the modes, the  $m = 1$  displacement of the plasma column has a toroidal shape similar to an interference pattern, with a maximum at an angle  $\varphi_L$  which is taken as the definition of the locking position [44]. The locking strength can be thought as a measure of the dispersion in the distribution of the phases of the  $m = 1$  perturbation to the radial magnetic field,

$$\sigma(\varphi) = \frac{1}{1 + 2 + \dots + (N - 1)} \times \sum_{j=n_1}^{n_2-1} \sum_{k=j+1}^{n_2} \cos(\Phi_{1,j} - \Phi_{1,k}), \quad (5)$$

considering  $N = (n_2 - n_1)$  harmonics with periodicity  $\Phi_{1,n} = \theta - n\varphi + \phi_{1,n}$ . Where the phases are closely aligned, almost zeroing the cosine arguments, the function  $\sigma(\varphi)$  has a maximum. In figure 7(b) the maximum value of  $\sigma(\varphi)$ , corresponding to  $\sigma(\varphi_L)$ , is plotted in time for  $n_1 = 8$ ,  $n_2 = 24$ . It can be seen that  $\sigma$  monotonically increases in  $[t_0, t_2]$ , reaching a saturation value  $\sigma \sim 0.9$ .

Summarizing this section, the  $m = 1$  and  $m = 0$  mode dynamics follows the same timing as the mean current redistribution. This allows the interpretation of DREs as a multitude of reconnection events starting in the core as  $m = 1$  and propagating towards the edge, where the process undergoes a transition to  $m = 0$  reconnection with  $J_{\parallel} = J_{\theta}$  following the  $q$  profile.

### 3. Magnetic topology evolution and a possible trigger of reconnection

In the previous section the typical temporal scales of the reconnection process have been identified, using edge measurements. Here the important spatial scales that could be at the origin of the reconnection process are identified studying the magnetic topology evolution before the onset of the DRE. We focus now on the reconstruction techniques of the magnetic topology in the whole plasma volume consistently with experimental boundary conditions, and to the definition of a

helical equilibrium capable of describing SH states prior to the DRE.

#### 3.1. Representation of the magnetic topology based on axisymmetry of the equilibrium

The magnetic topology related to tearing instabilities, which break the axisymmetry of the equilibrium magnetic field, is reconstructed in the whole plasma volume using a perturbative approach [42]. Newcomb's equations, arising from the force-free balance equation together with Ampère's law, are solved consistently with boundary conditions from edge magnetic measurements. Both external (with respect to the vacuum vessel) and internal magnetic measurements from the ISIS coil system are used for the computation. The solution returns the radial profile of the complex harmonics of the magnetic fluxes at a fixed time. Due to the limited set of experimental boundary conditions, the  $m = -1, 0, 1, 2$  spectra with  $n \leq 24$  are solvable in RFX-mod.

The topology of the magnetic field  $\mathbf{B}$  is explored by Poincaré plots based on Newcomb's reconstruction and on the whole MHD spectra [45]. In figure 9, Poincaré plots of  $\mathbf{B}$  are shown in the  $r-\varphi$  plane at  $\theta = 0$ , for selected times in the interval  $[-2.4, -0.2]$  ms during the evolution of the averaged discharge. The arrow in the first panel indicates the radial range of the reconstructed  $m = 1$  resonant flux surfaces, between  $q = 1/7$  and  $q = 1/24$ . At earlier times, Poincaré plots clearly show the helical magnetic structure dominating in the plasma core typical of SHAx states. Before the DRE (for  $t < t_1$ ), small amplitude secondary modes are responsible for the non-perfectly conserved flux surfaces inside the helix, for the stochastic volumes around them and for all the small islands that appear in the plasma; during the DRE, the increase of their amplitude (for  $t > t_1$ ) is responsible for the increase in magnetic chaos that gradually destroys the helical core. For  $t > t_2$  the amplitude of the dominant mode drops below the threshold for the existence of a single helical axis (SHAx states), and an island chain with the periodicity of the dominant mode can be recognized in the plasma core (dark blue in the plots). At  $t = t_2$  the plasma volume is almost all stochastic and at  $t = t_3$  just small  $m = 1, n = 7$  islands are still present in the plasma core. Note that, due to the Shafranov shift, the magnetic axis around which magnetic islands develop is located at small but positive radius. The edge  $m = 0$  island chain always separates the plasma from the wall, and a clear, localized,  $m = 0$  structure is visible in the edge region in  $[t_2, t_5]$  (here plotted in

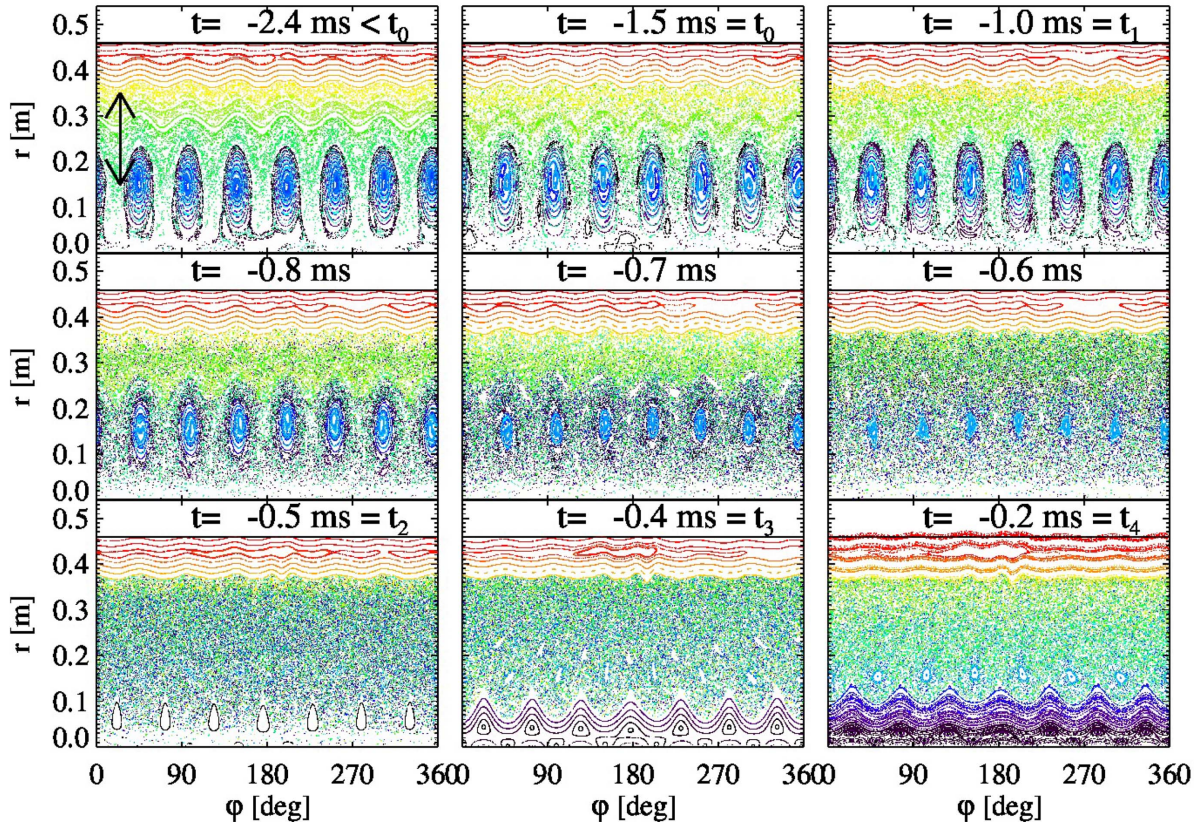


**Figure 9.** Averaged discharge. Poincaré plots in the  $(r-\varphi)$ -plane at  $\theta = 0$ , for times in the interval  $[-2.4, -0.2]$  ms. The arrow in the first panel indicates the radial range of the reconstructed  $m = 1$  resonant flux surfaces, between  $q = 1/7$  and  $q = 1/24$ .

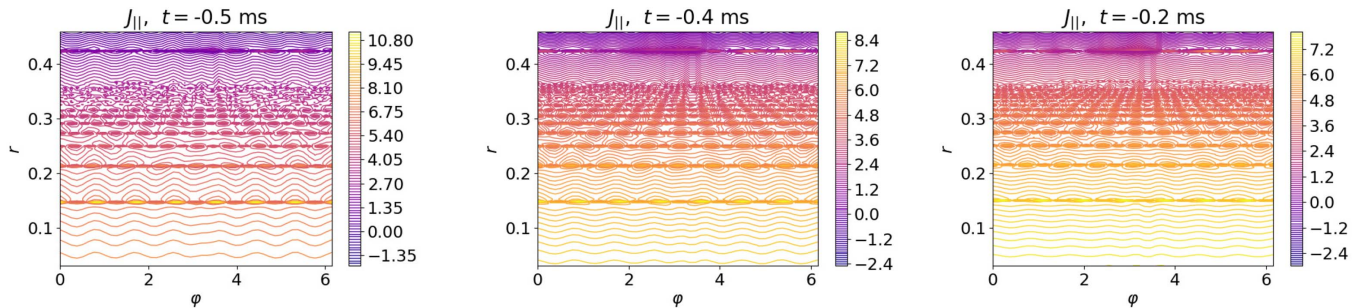


**Figure 10.** Averaged discharge. Contour plots of  $J_{\parallel}$  in the  $(r-\varphi)$ -plane at  $\theta = 0$ , for times  $[t_2, t_3, t_5] = [-0.5, -0.4, -0.2]$  ms.

red). The  $m = 1$  spectrum is rapidly decreasing with  $n$ , being high- $n$  modes less favorable due to very high distortion of the magnetic field lines. We therefore expect that the reconstruction of  $n \geq 24$  modes would show a larger area of non perfectly conserved flux surfaces at the edge, bringing magnetic chaos more near the  $m = 0$  island chain that interrupts the chaotic topology in the reversal region [46], without significantly change the results.

Contour plots of the total parallel current density  $J_{\parallel}$  are particularly relevant for the purpose of exploring the magnetic topology. A warning is in order before showing the representation of  $J_{\parallel}$  calculated as the curl of the magnetic field. Very small discontinuities around the resonant surfaces can be indeed uncovered if the magnetic field from Newcomb's calculations is visualized in detail. Even though the

representation of  $\mathbf{B}$  is still accurate enough, this is critical for the current density because the discontinuities fix the resonant current layers on the resonant flux surfaces defined by the unperturbed axisymmetric  $q$  profile, which is not appropriate to describe the first helical stages of the reconnection process (see next section for a more appropriate description of the helical equilibria, and [47] for a more extensive discussion on helical spectra). Contour plots of  $J_{\parallel}$  are anyway presented in figure 10 for  $t \in [t_2, t_5]$ . Since the helical deformation is small at the edge, the reversal surface is well defined even adopting an axisymmetric description and the attention may be posed on the  $m = 0$  structures. Note the clear  $m = 0$  current sheet that forms in the plasma in  $[t_2, t_3]$  at  $\varphi \sim \pi$ , in agreement with figures 6–8 and the locking position. The dominant  $m = 1$  mode is visible in the plasma core as a current structure

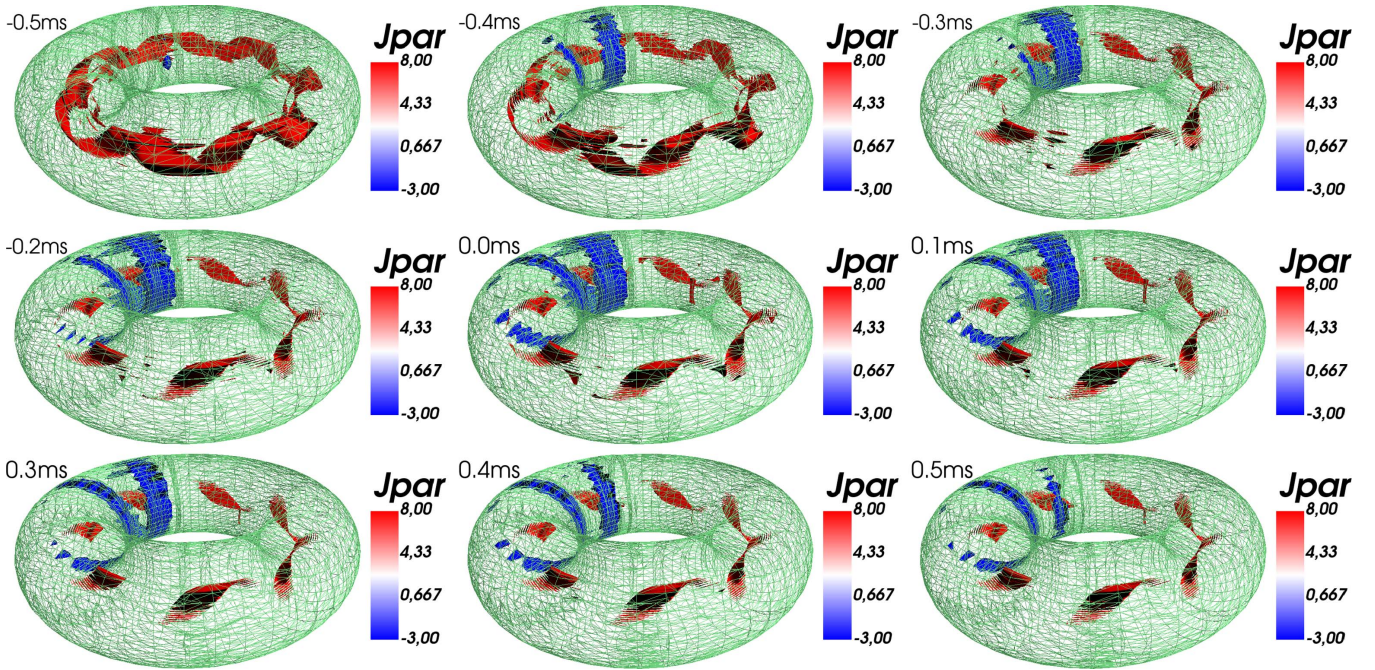


**Figure 11.** Averaged discharge. 3D plots of  $J_{\parallel}$ , together with the reversal surface (in green), at some instants in the interval  $[t_2, t_6] = [-0.5, +0.5]$  ms.

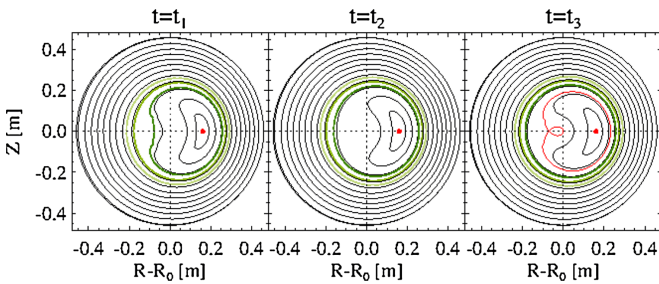


**Figure 12.** Averaged discharge. Contour plot at  $\varphi_{\text{fix}} = 45^\circ$  of the equilibrium magnetic flux surfaces in the SH approximation. Helical resonant surfaces with the periodicity of the  $m = 1, n = 8 - 10$  harmonics are highlighted in green. At  $t = t_3$  the flux surface in red is the separatrix of the  $m = 1, n = 7$  island. A red dot indicates the helical magnetic axis in SHAx states or the island O–point in DAX states, which corresponds to the  $\rho = 0$  coordinate in figure 13.

that develops on the  $m = 1, n = 7$  axisymmetric resonant surface. In the intermediate radii, between the innermost resonant (dominant) mode and the reversal surface, many current density structures arise with an  $n$ th-periodicity that follows, on the axisymmetric  $q$ -profile, the resonance positions of the  $m = 1$  spectrum: these structures are the resonant current sheets that generate the  $m = 1$  magnetic islands, which are not visible in the Poincaré plots due to their overlapping and the consequent magnetic chaos. Moreover, the contours clearly reveal mode locking, with all secondary modes in phase at  $\varphi = \pi$ , fully developed at  $t = t_2$  in agreement with figure 7(b). Due to magnetic chaos, mode locking is much less visible in Poincaré plots. No structures in the currents can be seen in the plots for  $r \in [0.35, 0.42]$ , simply because only  $m = 1$  modes up to  $n = 24$  are reconstructed in RFX–mod, which is resonant at  $r \sim 0.35$  as one can see in figure 4. The reconstruction of higher- $n$  modes

would show the corresponding resonant layers for  $r \geq 0.35$ , nevertheless, as discussed for the Poincaré plots, edge magnetic topology is expected not to change much due to high- $n$  modes.

A 3D visualization of the total parallel current density is proposed in figure 11, for selected times in  $[t_2, t_6] = [-0.5, +0.5]$  ms. The reversal surface, defined as the surface where  $q = 0$ , is shown in green. Attention can be paid to the time evolution of the helical structure of the dominant mode in the core and to the localized  $m = 0$  current sheet associated to the last sequences of the DRE. As already noted, the  $m = 0$  current sheet appears mostly as a  $n = 1$  and develops in the short  $[t_2, t_3]$  time interval ( $\sim 0.1$  ms). It first gains strength at the expense of the  $m = 1$  modes and then the diffusion of the current sheet brings to the end the reconnection process (for  $t > t_5$ ).

### 3.2. Magnetic topology reconstruction based on a single dominant mode

Using Newcomb’s solutions, a new helical equilibrium can be defined to model helical SHAx states prior to the DRE, originating from a single Fourier harmonic (SH approximation). Through this approximation that neglects secondary modes, a symmetry is recovered in the plasma and the helical flux surfaces [48] and the corresponding helical safety factor profile [49] can be defined.

*Evolution of the helical flux surfaces.* The evolution of the magnetic equilibrium is followed through the time evolution of the magnetic flux surfaces and of the safety factor profile. In the sequence of events of the DRE the magnetic configuration goes from SHAx to MH states, and, correspondingly, the best equilibrium approximation goes from

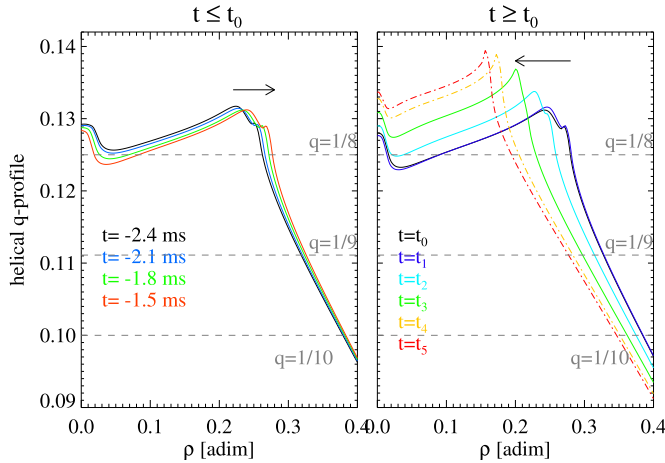


**Figure 13.** Averaged discharge. Zoom of the helical  $q$ -profile in the core region of the plasma, as a function of  $\rho$ . Left panel: evolution of the helical configuration during the almost stationary QSH phase that precedes the DRE ( $t < t_0$ ). Right panel: the helical safety factor profile during the DRE, reconstructed at the  $t_i$  time instants listed in section 2.2. Dashed lines are used for  $t > t_3$  because the axi-symmetric  $q_0$ -profile is a better choice to describe MH states. Horizontal lines highlight the position of the innermost helical resonances ( $q = 1/8$ ,  $q = 1/9$  and  $q = 1/10$ ).

the ideal helical symmetry to the ideal RFP axisymmetric equilibrium.

In figure 12, the contour plot of the magnetic flux surfaces in the SH approximation at some representative time instants shows this evolution on a fixed toroidal cross section. The toroidal angle is chosen such that the helical deformation is maximum on the equatorial plane at  $Z = 0$  ( $\varphi_{\text{fix}} = 45^\circ$ ). It can be noted that the helical deformation is maximum in the core region, decreasing outside, where it is relatively small with respect to the axi-symmetric circular boundary. Referring to the  $t_i$  time instants listed in section 2.2 and table 2, SHAx states are found for  $t < t_2$  and MH states for  $t > t_3$ ; in  $[t_2, t_3]$  the magnetic configuration passes from a SHAx state, with no separatrix and a clear single helical axis indicated by a red dot, to a DAx state, where the separatrix flux surface of the  $m = 1, n = 7$  magnetic island can be seen in the core region. The helical axis in this case corresponds to the island O-point. Then, for  $t > t_3$ , an axisymmetric description of the equilibrium is more suited to model MH states. In both cases, during helical or axisymmetric states, the addition of many MHD modes breaks the ideal symmetry and their role for the magnetic topology is illustrated in the Poincaré plots (figure 9), where the increasing magnetic chaos is evident during the DRE.

*Evolution of the helical safety factor profile.* Using the SH approximation, the safety factor profile is computed following a Hamiltonian approach [49]. As we will see in the following, the ensuing helical  $q$ -profile is not monotonically decreasing with the radius, the region between the helical axis and its maximum being related with the amplitude of the helical structure in the core. The innermost helical resonances are related to the  $m = 1, n = 8, 9, 10, \dots$  helical harmonics and  $m = 0$  modes are still resonant on the reversal surface.

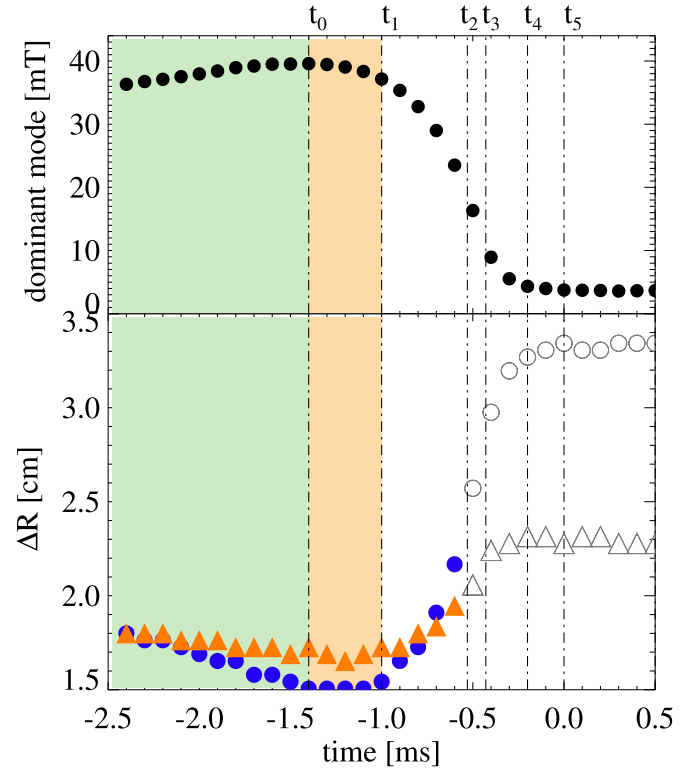


**Figure 14.** Averaged discharge. Top: time evolution of the maximum amplitude of the dominant mode  $m = 1, n = 7$ . Bottom: time evolution of the distance between the helical resonances  $m = 1, n = 8$  and  $m = 1, n = 9$  (blue) and  $m = 1, n = 9$  and  $m = 1, n = 10$  (orange). Gray color is used for  $t > t_2$  to remind the poorer characterization of the MH states using the helical  $q$ -profile instead of the axi-symmetric one.

In figure 13 the evolution of the helical safety factor profile is used to interpret the evolution of the magnetic configuration, with a special interest in the first stages when the reconnection process is being approached and a clear helical symmetry is present in the plasma. Helical  $q$  profiles are plotted as a function of the radial coordinate  $\rho$ , defined as the square root of the normalized helical flux, which is zero on the helical axis and one on the first wall [48]. Note that only the core region is reported in the figure. In the left panel the evolution of the helical configuration is shown for  $t < t_0$ , which corresponds to the almost stationary QSH phase that precedes the DRE. In the right panel the  $q$  profile is plotted during the DRE at the  $t_i$  time instants. A slow evolution of the helical equilibrium can be seen for  $t < t_0$ , with a slight increase of the plasma region between  $\rho = 0$  and the maximum of the safety factor profile. Correspondingly, there is a slight enlargement of the helical structure in the plasma core, as can be inferred also from the slight increase of amplitude of the dominant mode plotted in figure 14 (top). The resonant flux surfaces of the innermost tearing modes, following the slight increase of the dominant mode, move towards larger radii. In contrast, as indicated by the arrows in the figure, for  $t > t_0$  the crash of the dominant mode shrinks the helical structure in the core and brings backward the radial position of the innermost helical resonances.

*Consequences on the helical resonances - and the trigger of the reconnection event.* There is a strict relation between

this evolution and that of the radial distance among the helical resonant flux surfaces, see figure 14 (bottom) for the three innermost helical resonances  $q = 1/8$ ,  $q = 1/9$  and  $q = 1/10$ . The distances are computed on the outboard midplane at  $Z = 0$  and  $\varphi = \varphi_{\text{fix}}$ , where magnetic flux surfaces are closer due to the helical deformation (see figure 12). During the almost stationary QSH phase that precedes the DRE ( $t < t_0$ ), the  $m = 1$  helical resonances, while moving slowly towards larger radii, approach each other. At  $t = t_0$  the radial distance between  $m = 1$  resonances is minimum and the MHD modes start locking in phase (figure 7). Their radial distance keeps almost constant until  $t = t_1$ , when the fast stages of the reconnection process start. During reconnection there is a strong change in magnetic configuration and the distances between resonances quickly increase between  $t = t_1$  and  $t = t_3$ , although their significance is blurred by the poorer characterization of the MH states using the helical  $q$ -profile, as indicated by gray color in the figure.

It is worth emphasizing that the measurements shown in figures 5–8 do not show any significant variation for  $t < t_0$ . A significant change can be inferred only after performing detailed calculations of the initial evolution of equilibria, although consistent with the magnetic measurements. We conclude that a slight modification of the helical equilibrium before the DRE ( $t < t_0$ ), which pushes closer together the principal resonances in the plasma core and peaks the parallel current density, may be responsible for the triggering of the reconnection.

#### 4. Discussion

Developing a common picture of the reconnection events in laboratory and even astrophysical plasmas could help in understanding the physics (and maybe mitigating or even stimulating the effect) of these explosive events. Mentioning for example [50–52], the trigger, the rate and the energetics problems are keys in much reconnection research.

In this paper, the trigger of the reconnection has been identified with topological features, and in particular with the proximity of some reconnection sites that get closer in the plasma core. The approaching of magnetic islands developing on resonant surfaces can end up with magnetic chaos (Chirikov criterion [53]), which is probably the typical background in RFP reconnections and could also be responsible for their trigger in the high plasma current discharges discussed here. The relationship between the tearing-mode current sheets (responsible for the opening of magnetic islands) and the reconnecting current sheet (responsible for the DRE event) is an interesting point to be explored, maybe in relation with the plasmoid instability that could characterize the tearing-mode current sheets for high values of the Lundquist number ( $S > 10^4$  or even smaller in a stochastic background) [54].

Different reconnection rates are expected varying the position in the  $(L, S)$  parameter space (with  $L$  the effective plasma size [55]). Some effort should be done to extend the studies reported in this paper to different values of the plasma current (hence  $S$ ) and the equilibrium parameter  $F$ , enriching the phase

diagram of reconnection events with RFX-mod experience. A scan in the equilibrium reversal parameter  $F$  could give some insight on the presence of different types of reconnection events, as those observed in the RFP MST experiment [56], with probably different reconnection rates. Moreover, magnetic reconnection may be influenced and determined both by local plasma dynamics in the reconnection region and global boundary conditions [57], which in turn may alter the current density profile. The relation between the DRE dynamics in discharges with and without externally applied magnetic perturbations should be studied as well [58].

An important part of the energetic problem is the appearance of non-thermal energetic particles. Further work is needed to investigate the relationship between the spatial distribution of the heating and the spatial location of the reconnection, as done e.g. in [59]. In RFX-mod2 [60] dedicated diagnostics will be available by means of a charge-exchange recombination spectroscopy system. New dedicated diagnostics will be available with the aim of determining during the reconnection process, with space and high time resolution, the dynamics of the neutron flux generated by DD fusion reaction, whose enhancement is sign of ion acceleration and/or heating [61].

Finally, it is worth recalling that energy transport barriers related to SHAx states do not last for as long as the magnetic structure [62], with the crash of the electron temperature gradient preceding the magnetic one. The relation between thermal transport barriers in SHAx states and the position of the helical resonances has to be further investigated to interpret the electron temperature dynamics before magnetic reconnection events, as done in [63] in the case of SHAx state formation.

#### 5. Conclusions

A phenomenological description of global discrete relaxation events (DREs) typical of high plasma current discharges in RFX-mod is the subject of this paper. To this aim, an averaged discharge with reference plasma current of 1.5 MA is used for the analysis. Roughly speaking, an initial almost stationary SHAx state, characterized by a helical deformation of the plasma column, heads for a DRE that destroys this symmetry giving rise to a more chaotic MH state with broad MHD spectrum.

DREs are associated to reconnection events, and spatial and temporal scales are invoked as fundamental observables. A list of time instants (table 2) has been defined to describe the temporal sequence of the reconnection process.

$t < t_0$ : Before the DRE helical states are considered almost stationary, with the dominance of the innermost resonant mode, very low amplitude of secondary modes and electromagnetic measurements that show an almost stationary phase. Helical equilibrium reconstructions suggest a possible trigger of the reconnection process, which has been associated to a tiny growth of the helical structure, that brings the main core helical resonances closer together.

$t_0 < t < t_1$ : It is suggested that the interaction between radially distributed tearing modes and related current sheets is at the origin of the reconnection process: when helical resonances reach their minimum distance (at  $t = t_0$ ), it starts the phase locking of the  $m = 1$  modes that aligns all the harmonics in some position. Reconnection starts there, where the kink perturbation is maximum.

$t > t_1$ : A sequence of fast reconnection stages corresponds then (for  $t > t_1$ ) to the growth of the secondary  $m = 1$  and  $m = 0$  mode amplitudes. The accord between the timings of the MHD mode dynamics and the current density redistribution, suggests the interpretation of a reconnection process starting in the core as  $m = 1$  reconnections ( $t = t_1$ ) and propagating towards the edge ( $t = t_2$ ), where the process turns into  $m = 0$  reconnection ( $t = t_3$ ) where  $J_{\parallel} = J_{\theta}$ .

The evolution of the magnetic topology has been followed by means of Poincaré plots based on Newcomb's reconstructions. Magnetic chaos due to the overlapping of the  $m = 1$  magnetic islands complicates the picture of interacting current layers, and the trigger of the reconnection could implicate some degree of magnetic chaos due to the presence of small amplitude secondary modes even before the DRE—but this is beyond the scope of this paper.

## ORCID iDs

B. Momo  <https://orcid.org/0000-0001-7760-8960>  
 H. Isliker  <https://orcid.org/0000-0001-9782-2294>  
 R. Cavazzana  <https://orcid.org/0000-0002-1651-1070>  
 M. Zuin  <https://orcid.org/0000-0002-0282-2978>  
 L. Cordaro  <https://orcid.org/0000-0002-8068-5307>  
 D. Lopez-Bruna  <https://orcid.org/0000-0002-7638-8772>  
 E. Martinez  <https://orcid.org/0000-0002-4181-2959>  
 I. Predebon  <https://orcid.org/0000-0002-2100-4698>  
 C. Rea  <https://orcid.org/0000-0002-9948-2649>  
 M. Spolaore  <https://orcid.org/0000-0002-2350-2033>  
 L. Vlahos  <https://orcid.org/0000-0002-8700-4172>

## References

- [1] Biskamp D. 2000 *Magnetic Reconnection in Plasmas* (Cambridge, New York: Cambridge University Press)
- [2] Wesson J. 2004 *Tokamaks* 3rd ed (New York: Oxford)
- [3] Lopez Bruna D. et al 2013 Relationship between MHD events, magnetic resonances and transport barriers in TJ-II plasmas *Nucl. Fusion* **53** 073051
- [4] Cappello S. and Biskamp D. 1996 Reconnection processes and scaling laws in reversed field pinch magnetohydrodynamics *Nucl. Fusion* **36** 571
- [5] Ortolani S. and Schnack D.D. 1993 *Magnetohydrodynamics of Plasma Relaxation* (Singapore: World Scientific Publishing)
- [6] Finn J.M., Nebel R. and Bathke C. 1992 Single and multiple helicity Ohmic states in reversed-field pinches *Phys. of Fluids B: Plasma Phys.* **4** 1262
- [7] Cappello S. 2004 Bifurcation in the MHD behaviour of a self-organizing system: the reversed field pinch (RFP) *Plasma Phys. Control. Fusion* **46** 313
- [8] Bonfiglio D. et al 2005 Dominant Electrostatic Nature of the Reversed Field Pinch Dynamo *Phys. Rev. Lett.* **94** 145001
- [9] Cappello S. et al 2006 Magnetohydrodynamic dynamo in reversed field pinch plasmas Electrostatic drift nature of the dynamo velocity field *Phys. Plasmas* **13** 056102
- [10] Cappello S. and Escande D.F. 2000 Bifurcation in viscoresistive MHD: the Hartmann number and the reversed field pinch *Phys. Rev. Lett.* **85** 3838
- [11] Escande D.F. et al 2000 Quasi-single-helicity reversed-field-pinch plasmas *Phys. Rev. Lett.* **85** 8
- [12] Marrelli L. et al 2002 Quasi-single helicity spectra in the Madison symmetric torus *Phys. Plasma* **9** 2868
- [13] Franz P. et al Tomographic imaging of resistive mode dynamics in the Madison symmetric torus reversed-field pinch *Phys. Plasma* 2006 **13** 012510
- [14] Frassinetti L. et al 2007 Spontaneous quasi single helicity regimes in EXTRAP T2R reversed-field pinch *Phys. Plasma* **14** 112510
- [15] Piovesan P. et al 2004 Self-organization towards helical states in the Toroidal Pinch Experiment reversed-field pinch *Phys. Plasmas* **11** 151
- [16] Martin P. et al 2003 Overview of quasi-single helicity experiments in reversed field pinches *Nucl. Fusion* **43** 855
- [17] Piovesan P., Zuin M. et al 2009 Magnetic order and confinement improvement in high-current regimes of RFX-mod with MHD feedback control *Nucl. Fusion* **49** 085036
- [18] Lorenzini R. et al Self-organized helical equilibria as a new paradigm for ohmically heated fusion plasmas *Nat. Phys.* **5** 570
- [19] Lorenzini R. et al 2008 Single-helical-axis states in reversed-field-pinch plasmas *Phys. Rev. Lett.* **101** 025005
- [20] Martin P. et al 2009 Overview of RFX-mod results *Nucl. Fusion* **49** 104019
- [21] Carraro L. et al 2009 Improved confinement with internal electron transport barriers in RFX-mod *Nucl. Fusion* **49** 055009
- [22] Lorenzini R. et al 2012 On the energy transport in internal transport barriers of RFP plasmas *Nucl. Fusion* **52** 062004
- [23] Puiatti M.E. et al 2009 Helical equilibria and magnetic structures in the reversed field pinch and analogies to the tokamak and stellarator *Plasma Phys. Control. Fusion* **51** 124031
- [24] Fitzpatrick R. and Zanca P. 2002 Phase-locking of tearing modes in the reversed field experiment *Phys. Plasmas* **9** 2707
- [25] Lorenzini R. et al 2007 Toroidally asymmetric particle transport caused by phase-locking of MHD modes in RFX-mod *Nucl. Fusion* **47** 11
- [26] Innocente P. et al 2000 Magnetic relaxation and discrete dynamo action in RFX 27th Conf. on Contr. Fusion and Plasma Phys (Budapest, Hungary 12–16 June 2000) vol 24B pp 1360–3 ([http://epsppd.epfl.ch/Buda/pdf/p4\\_026.pdf](http://epsppd.epfl.ch/Buda/pdf/p4_026.pdf))
- [27] Zuin M. et al 2009 Current sheets during spontaneous reconnection in a current-carrying fusion plasma *Plasma Phys. Control Fusion* **51** 035012
- [28] Sonato P. et al 2003 Machine modification for active MHD control in RFX *Fusion Eng. Des.* **66** 161
- [29] Piovesan P. et al 2013 RFX-mod: a multi-configuration fusion facility for three-dimensional physics studies *Phys. Plasmas* **20** 056112
- [30] Sonato P., Piovani R., Lucchetta A. and RFX-mod team 2005 Control of non-axisymmetric magnetic fields for plasma enhanced performances: The RFX contribution *Fusion Eng. Des.* **74** 97
- [31] Martini S. et al 2007 Active MHD control at high currents in RFX-mod *Nucl. Fusion* **47** 783–791
- [32] Zanca P. et al 2007 Beyond the intelligent shell concept: the clean-mode-control *Nucl. Fusion* **47** 1425

- [33] Paccagnella R. *et al* 2006 Active-feedback control of the magnetic boundary for magnetohydrodynamic stabilization of a fusion plasma *Phys. Rev. Lett.* **97** 075001
- [34] Bolzonella T. *et al* 2008 Resistive-wall-mode active rotation in the RFX-Mod device *Phys. Rev. Lett.* **101** 165003
- [35] Valisa M. *et al* 2008 High current regimes in RFX-mod *Plasma Phys. Control. Fusion* **50** 124031
- [36] Serianni G. *et al* 2004 Development, tests, and data acquisition of the integrated system of internal sensors for RFX *Rev. Sci. Instrum.* **75** 4338
- [37] Paccagnella R. 1998 Linear magnetohydrodynamic stability in reversed field pinch with distant and multiple resistive wall *Nucl. Fusion* **38** 7
- [38] Ejima S., Callis R.W., Luxon J.L., Stambaugh R.D., Taylor T.S., Wesley J.C. 1982 Volt-second analysis and consumption in doublet III plasmas *Nucl. Fusion* **22** 10
- [39] Cavazzana R. 2019 Electromagnetic modelling of the Reversed Field Pinch configuration *Proc. of 46th Conf. on Plasma Physics* (Milan, Italy, 8–12 July 2019) P1.1052 (<http://ocs.ciemat.es/EPS2019PAP/pdf/P1.1052.pdf>)
- [40] Cavazzana R. 2018 Dissipative loop voltage of the RFP configuration *Technical note FB-NT-115*
- [41] Spagnolo S. *et al* 2011 Alfvén eigenmodes in the RFX-mod reversed-field pinch plasma *Nucl. Fusion* **51** 083038
- [42] Zanca P. and Terranova D. 2004 Reconstruction of the magnetic perturbation in a toroidal reversed field pinch *Plasma Phys. Control Fusion* **46** 1115–1141
- [43] Robertson S. and Green P. 1993 Locking of kink modes in a reversed field pinch *Phys. Fluids B* **5** 550
- [44] Zanca P. *et al* 2001 Analysis of phase locking of tearing modes in reversed field pinch plasmas *Phys. Plasma* **8** 516
- [45] Innocente P. *et al* 2017 FLiT: a field line trace code for magnetic confinement devices *Plasma Phys. Control. Fusion* **59** 045014
- [46] Spizzo G., White R.B and Cappello S. 2007 Chaos generated pinch effect in toroidal confinement devices *Physic. Plasma* **14** 102310
- [47] Predebon I. *et al* 2016 MHD spectra and coordinate transformations in toroidal systems *Physic. Plasma* **23** 092508
- [48] Martinez E. *et al* 2011 Equilibrium reconstruction for single helical axis reversed field pinch plasmas *Plasma Phys. Control Fusion* **53** 035015
- [49] Momo B. *et al* 2011 Magnetic coordinate systems for helical SHAx states in reverse field pinch plasmas *Plasma Phys. Control Fusion* **53** 125004
- [50] Zweibel E.G. and Yamada M. 2016 Perspectives on magnetic reconnection *Proc. R. Soc. A* **472** 20160479
- [51] Isliker H., Vlahos L. and Constantinescu D. 2017 Fractional transport in strongly turbulent plasmas *Phys. Rev. Lett.* **119** 045101
- [52] Isliker H., Pisokas T., Vlahos L. and Anastasiadis A. 2017 Particle acceleration and fractional transport in turbulent reconnection *Astrophys. J.* **849** 35
- [53] Chirikov B. 1979 A universal instability of many-dimensional oscillator systems *Physics Reports* **52** 263–379
- [54] Louriero N.F. and Uzdensky D.A. 2016 Magnetic reconnection: from the Sweet–Parker model to stochastic plasmoid chains *Plasma Phys. Control Fusion* **58** 014021
- [55] Ji H. and Daughton W. 2011 Phase diagram for magnetic reconnection in heliophysical, astrophysical, and laboratory plasmas *Phys. Plasmas* **18** 111207
- [56] Choi S. *et al* 2006 Cause of Sudden Magnetic Reconnection in a Laboratory Plasma *Phys. Rev. Lett.* **96** 145004
- [57] Bonfiglio D., Veranda M., Cappello S., Escande D.F. and Chacon L. 2013 Experimental-like helical self-organization in reversed-field pinch modeling *Phys. Rev. Lett.* **111** 085002
- [58] Bonfiglio D., Veranda M., Cappello S., Escande D.F. and Chacon L. 2015 Helical self-organization in 3D MHD modelling of fusion plasmas *Plasma Phys. Control Fusion* **57** 044001
- [59] Gangadhara S. 2007 Spatially resolved measurements of ion heating during impulsive reconnection in the Madison symmetric torus *PRL* **98** 075001
- [60] Zuin M. *et al* 2017 Overview of the RFX-mod fusion science activity *Nucl. Fusion* **57** 102012
- [61] Magee P. 2011 Anisotropic ion heating and tail generation during tearing mode magnetic reconnection in a high-temperature plasma *Rev. Lett.* **107** 065005
- [62] Franz P. *et al* 2013 Experimental investigation of electron temperature dynamics of helical states in the RFX-mod reversed field pinch *Nucl. Fusion* **53** 053011
- [63] Zhang Y. *et al* 2017 Thermal properties of three sub-states of quasisingle helicity states on RFX-mod *Plasma Phys. Control. Fusion* **59** 125002